Masters's Thesis

Material Characterization by Millimeter-Wave Techniques

Leonard Andersson

Department of Electrical and Information Technology,
Faculty of Engineering, LTH, Lund University, 2016.

Material Characterization by Millimeter-Wave Techniques

Department of Electrical and Information Technology-
Faculty of Engineering, LTH, Lund University
SE-221 00, Lund, Sweden

LUND
UNIVERSITY

Author:
Leonard Andersson

Supervisors:
Lars-Erik Wernersson
Sebastian Heunisch

Examiner:
Erik Lind

March 2016

Abstract

This master thesis investigates material characterization by reflection and transmission of electromagnetic waves in the 40-60 GHz band (millimeter-wave spectrum) for different materials. The free-space measurement method is a fast, efficient and non-destructive way of examining a material and is being researched by both academics and industries.

The theory of how electromagnetic waves interact with different materials such as dielectrics and conductors is reviewed as well as how the reflection and transmission from such materials can be computed theoretically. This theory is partially derived from Maxwell's equations. From this theory, simulations are performed to get signal levels of reflection and transmission for different materials and varying material parameters. From the simulations it is shown that certain materials are better examined in either transmission or reflection.

Measurements were performed in time domain (with a wavelet generator and an oscilloscope) and in frequency domain (with a network analyzer). Both reflection and transmission were measured for all samples. Four samples were investigated thoroughly: two PMMA (Poly(Methyl MethAcrylate)) samples, one silicon sample and a thin gold film sample.

Before the measured data can be compared to the simulated, it is necessary to apply signal processing to both the measured and the simulated data. This is done to make sure the comparison of the two data sets works and it consists of removing multiple reflections and other unwanted noise from the signal. The material characterization could then be performed, by extracting a specific material parameter, such as permittivity or conductivity. This is done by comparing simulated data iteratively to measured data. The best fit should then, in theory, correspond to the actual material parameter.

The material characterization worked, although sometimes differences in time and frequency domain were found. Permittivity values were extracted for the PMMA samples and conductivity values for the silicon and thin gold film samples. The values extracted compared well with reference values for the PMMA samples and the thin gold film sample.

Contents

CHAPTER 1

1 Introduction

This thesis was a part of the final project examination for the degree *Master of Science in Engineering Nanoscience* from Lund University, Lund, Sweden. The work presented here was performed with the Nanoelectronics Group at the Department of Electrical and Information Technology, Lund University.

1.1 Background & Motivation

The recent advancement of material characterization by time- or frequency domain measurements has received a lot of attention lately because of its non-destructive, fast and efficient way of probing a material. Research in this area confirms that free-space probing by transmission and reflection measurements makes it possible to calculate the complex permittivity of a material and thereby decide its composition, without being in contact with the material.

It is known that the dielectric properties of a material corresponds to different material characteristics and recent research also shows that this relation can be used to determine not only electrical conductivity, permittivity and permeability but also properties such as chemical concentration, moisture content, bulk density, bio-content and stress-strain relationship. This is not only interesting for the scientific community but also for the industrial world. This technology could be useful in food science, medicine, agriculture, chemistry, defense industry, electrical devices, biology and civil engineering [1] [2].

One of the main challenges today is to accurately measure the material properties of thin samples (100 to 1000 nm range). Many methods exist for measuring these properties, such as parallel plate capacitors, transmission-line/waveguides methods or free space methods. For higher frequencies, where the wavelength is roughly a millimeter, free space methods are favored. This is because if the wavelength is smaller than the sample, one can neglect effects such as diffraction and charge buildup at the edges of the sample [3] [5].

1.2 Project Description

The aim with this Master's thesis was to study reflection and transmission of millimeter-wave wavelets propagated through dielectrics and absorbing materials with conductivity and/or permittivity. The materials investigated were, among others, silicon-wafers and dielectrics. Further work could look at materials such as organic solar cells and thin film dielectrics with semiconducting nanostructures. The thesis includes reference measurements on known material as well as measurements on new materials. The work also contains modeling and simulations of material properties and their effect on transmission and reflection.

1.3 Methodology

The methodology used can be divided into two steps. First, models were chosen to describe how electromagnetic waves interact with materials and simulations of these models were implemented. Second, measurements in time and frequency domain were performed and data collected. This data was examined and its consistency with the simulations were evaluated.

1.4 Outline of the report

This master's thesis starts with a thorough review of the theory behind reflection and transmission from electromagnetic waves impinging upon different kind of materials, as well as material models for conductors and dielectrics in Chapter 2. Chapter 3 explains the methodology used, as well as how and why the simulations were done. In Chapter 4 the results are discussed and analyzed. Finally, chapter 5 draws conclusions and summarizes the whole report.

CHAPTER 2

2 Theoretical background

The theoretical background of this report is electromagnetic wave propagation and the electrodynamics of solids, which is a vital cornerstone for understanding the simulations, measurements and conclusions.

The theory and statements in this chapter are mainly based on concepts covered in *Orfanidis* [4], *Dressel and Grunner* [5] and *Bishop* [6].

2.1 Maxwell's equations, permittivity and permeability

Between 1861 and 1862 James Clerk Maxwell published the famous Maxwell's equations (which in turn are based on Ampere's circuit law, Faradays law of induction, Gauss's law for magnetism and Gauss's flux theorem).

These integral equations, in combination with the law of the Lorentz force, formed the groundwork for classical electromagnetic theory and optics. In (1), Maxwell's equations are stated in SI-units.

$$\begin{aligned} \nabla \times \boldsymbol{E} &= -\frac{\partial \boldsymbol{B}}{\partial t} \\ \nabla \times \boldsymbol{H} &= \boldsymbol{J} + \frac{\partial \boldsymbol{D}}{\partial t} \\ \nabla \cdot \boldsymbol{D} &= \rho \\ \nabla \cdot \boldsymbol{B} &= 0. \end{aligned} \tag{1}$$

The following derivation of equations follows that of reference [4]. The four different vectors on the left-hand side in (1), the electric and magnetic field intensities $\boldsymbol{E}, \boldsymbol{H}$ and the flux densities $\boldsymbol{D}, \boldsymbol{B}$ are related to each other by constitutive relations.

Equation (2) shows these constitutive relations in their most simple form (for vacuum):

$$\boldsymbol{D} = \varepsilon_0 \boldsymbol{E}$$
$$\boldsymbol{B} = \mu_0 \boldsymbol{H}. \tag{2}$$

The two constants combining these quantities, ε_0 and μ_0, are the permittivity and permeability of vacuum. With the permittivity and permeability of vacuum we can define the speed of light in vacuum and the characteristic impedance of vacuum: $c_0 = 1/\sqrt{\varepsilon_0 \mu_0}$ and $\eta_0 = \sqrt{\mu_0/\varepsilon_0}$.

The same constitutive relations can be written for materials. For a homogeneous isotropic material they are:

$$\boldsymbol{D} = \varepsilon \boldsymbol{E}$$
$$\boldsymbol{B} = \mu \boldsymbol{H} \tag{3}$$

Where ε and μ is the materials absolute permittivity and permeability. By dividing the materials permittivity and permeability by its respective vacuum equivalent, one can define the relative permittivity and permeability:

$$\varepsilon_r = \frac{\varepsilon}{\varepsilon_0}, \qquad \mu_r = \frac{\mu}{\mu_0} \tag{4}$$

The refractive index of a material (5) is defined as the square root of the relative permittivity multiplied with the relative permeability:

$$n = \sqrt{\varepsilon_r \mu_r} \tag{5}$$

By using the values of a material's permittivity and permeability, one can calculate the speed by which light travels in a material and the characteristic impedance of a material the same way as for vacuum. By using this fact together

with (4) and (5) one can obtain the useful relations in (6) and (7) with some substitutions and extrapolations:

$$\eta = \eta_0 \frac{\mu_r}{n} = \eta_0 \frac{n}{\varepsilon_r} \tag{6}$$

$$c = \frac{c_0}{n} \tag{7}$$

This master's thesis only examines non-magnetic materials, which means $\mu = \mu_0$, or $\mu_r = 1$ and (6) simplifies to $\eta = \eta_0/n$.

In general, the absolute permittivity ε is a complex quantity which can be expressed as

$$\varepsilon(\omega) = \varepsilon_0 \varepsilon_r(\omega) = \varepsilon'(\omega) - j\varepsilon''(\omega). \tag{8}$$

where $\omega = 2\pi f$ is the angular frequency and f the frequency. This can be understood by considering a dipole exposed to an alternating electric field. The dipole exposed to the field will rotate and try to align itself with it. After a certain time, the electric field reverses direction and the dipole must re-align with the field (to remain parallel to the correct polarity). As this oscillation occurs, the friction experienced by the dipole through the acceleration and deceleration of the rotation causes it to lose energy through heat generation. (This is also how microwave ovens work, the dipole in that case is polar water molecules [7]) The imaginary part of the permittivity is a measure of the degree to which the dipole is out of phase with the electric field. The resulting losses through heat therefore determine how large the imaginary permittivity is. A larger imaginary part indicates a lot of energy is being dissipated through heat. The imaginary part therefore directly reflects the loss in the material. [6]

A dipole is created when an imbalance of charge is present. For molecules this takes form in polar covalent bonds, where one or more atoms of the molecule have a higher electronegativity than the rest. This makes the electron cloud unevenly distributed across the molecule and creates a nonzero dipole moment. These molecules are known as polar molecules. Non-polar molecules (such as O_2) can, however, temporarily become dipoles under electric fields and therefore dissipate energy from the field. This happens because of the mass imbalance

between the positive nucleus and negative electron cloud. The lighter electron cloud will align much faster with the field and therefore a dipole is momentarily created [6] [8].

One possible way to model these properties is by the following equation:

$$m\ddot{x} = eE - kx - m\gamma\dot{x} \tag{9}$$

where $\dot{x} = dx/dt$, m is the electron rest mass and the electric field E is only present in the x-direction. This equation describes the force a bound or unbound electron experiences when exposed to an electromagnetic field. The kx factor comes from the desire of the negative electron to go back to its original state near the positive nucleus and the $m\gamma\dot{x}$ factor from any friction force, proportional to the electron-velocity. From Hooke's law [9] we know the constant k is linked to the resonance frequency, ω_0, of the (atomic)-spring by $\omega_0 = \sqrt{k/m}$. Rewriting (9) together with this fact gives:

$$\ddot{x} + \gamma\dot{x} + \omega_0^2 x = \frac{e}{m}E \tag{10}$$

Some interesting characteristics can immediately be seen in (10). When $\omega_0 = 0$ there is no force pulling the electrons to stay near the nuclei, therefore this case describes free moving electrons i.e. a conductor. The term $\gamma\dot{x}$ appears from collisions that, on average, slow the electron down. The γ parameter can therefore be interpreted as the rate of collisions per unit time, implying that $\tau = 1/\gamma$ is the mean-time between collisions.

2.1.1 Dielectrics

In dielectrics, $\omega_0 \neq 0$ and $\gamma \neq 0$, and if the electromagnetic field can be described as a sine wave, $E(t) = Ee^{j\omega t}$ with angular frequency ω, then the solution to (10) will be on the form of $x(t) = xe^{j\omega t}$. Inserting this and replacing the time derivatives by their frequency part $j\omega$ gives:

$$-\omega^2 x(t) + j\omega\gamma x(t) + \omega_0^2 x(t) = \frac{e}{m}E(t) \tag{11}$$

Rearranging the terms gives the final solution:

$$x(t) = \frac{\frac{e}{m}E(t)}{\omega_0^2 - \omega^2 + j\omega\gamma} \tag{12}$$

Following this and further mathematical steps, *"Orfanidis"* [4] defines the effective permittivity as:

$$\varepsilon(\omega) = \varepsilon_0 + \frac{\frac{Ne^2}{m}}{\omega_0^2 - \omega^2 + j\omega\gamma} \tag{13}$$

and by defining a material parameter called the plasma frequency, $\omega_p^2 = Ne^2/\varepsilon_0 m$, one can rewrite (13) in a more convenient form as:

$$\varepsilon(\omega) = \varepsilon_0 + \frac{\varepsilon_0\omega_p^2}{\omega_0^2 - \omega^2 + j\omega\gamma} \tag{14}$$

Materials that can be described by (14) are known as "Lorentz dielectrics". As stated above, the real and imaginary parts of the effective permittivity corresponds to two different phenomena. The real part is responsible for refractive properties and the imaginary part for absorptive properties. Following the convention set up in (8) one obtains:

$$\varepsilon'(\omega) = \varepsilon_0 + \frac{\varepsilon_0\omega_p^2(\omega_0^2 - \omega^2)}{(\omega^2 - \omega_0^2)^2 + \omega^2\gamma^2}, \qquad \varepsilon''(\omega) = \frac{\varepsilon_0\omega_p^2\omega\gamma}{(\omega^2 - \omega_0^2)^2 + \omega^2\gamma^2} \tag{15}$$

for the real and imaginary part respectively.

2.1.2 Conductors

The conducting characteristics of a material are described by Ohm's law:

$$\boldsymbol{J} = \sigma \boldsymbol{E} \tag{16}$$

This law can be derived from the "Lorentz dielectrics" model above. In *"Orfanidis"* [4] this derivation can be examined in detail. From this derivation, the conductivity can be expressed as:

$$\sigma(\omega) = \frac{j\omega\varepsilon_0\omega_p^2}{\omega_0^2 - \omega^2 + j\omega\gamma} \tag{17}$$

The similarity to (14) is obvious and a new way to state a materials effective permittivity is:

$$\varepsilon(\omega) = \varepsilon_0 + \frac{\sigma(\omega)}{j\omega} \tag{18}$$

As mentioned above, a metal have unbound conduction charges and therefore $\omega_0 = 0$. Simplifying (17) with this fact gives:

$$\sigma(\omega) = \frac{\varepsilon_0\omega_p^2}{\gamma + j\omega} \tag{19}$$

for a metal. This is known as the "Drude model".

2.1.3 Semiconductors

A material that exhibits both dielectric and conductivity properties (a semiconductor) can therefore be described by the sum of two terms; the first term describing bound charges and the second unbound charges [4]. Assigning different parameters $\{\omega_0, \omega_p, \gamma\}$ for each term, the total permittivity becomes:

$$\varepsilon(\omega) = \varepsilon_0 + \frac{\varepsilon_0 \omega_{dp}^2}{\omega_{d0}^2 - \omega^2 + j\omega\gamma_d} + \frac{\varepsilon_0 \omega_{cp}^2}{j\omega(\gamma + j\omega)} \tag{20}$$

Merging the first two terms as $\varepsilon_d(\omega)$ and the third as $\sigma_c(\omega)/j\omega$ one obtains

$$\varepsilon(\omega) = \varepsilon_d(\omega) + \frac{\sigma_c(\omega)}{j\omega} \tag{21}$$

which is the total effective permittivity of a material with both dielectric and conductive properties.

2.2 Uniform electromagnetic plane waves

One way of describing an electromagnetic wave is to assume a uniform plane sine wave, propagating along a fixed direction. At one frequency and in a lossless material such waves can be described by:

$$E(z,t) = E(z)e^{j\omega t}$$
$$H(z,t) = H(z)e^{j\omega t} \tag{22}$$

From superposition and the theory of electromagnetic fields we know that the electric- and magnetic field vectors can be described in terms of a forward and backwards moving field $E_{\pm}$:

$$E(z,t) = E_{+}(z,t) + E_{-}(z,t)$$
$$H(z,t) = \frac{1}{\eta}[E_{+}(z,t) - E_{-}(z,t)] \tag{23}$$

By following the derivations from *"Orfanidis"* [4], one obtains the general solution for a single-frequency wave expressed as the superposition of forward and backward components

$$E(z) = E_{0+}e^{-jkz} + E_{0-}e^{jkz}$$
$$H(z) = \frac{1}{\eta}\left[E_{0+}e^{-jkz} - E_{0-}e^{jkz}\right] \tag{24}$$

The reflection and transmission from uniform plane waves, with normal incidence, is discussed next.

2.2.1 Reflection and Transmission

Consider the uniform plane wave propagating in the z-direction in an isotropic and lossless material. If the field is linearly polarized in the x-direction, one gets

$$E(z) = E_{0+}e^{-jkz} + E_{0-}e^{jkz} = E_{+}(z) + E_{-}(z)$$
$$H(z) = \frac{1}{\eta}\left[E_{0+}e^{-jkz} - E_{0-}e^{jkz}\right] = \frac{1}{\eta}[E_{+}(z) - E_{-}(z)] \tag{25}$$

following the convention of (24). One can also express the backward and forward moving fields $E_{\pm}(z)$ in terms of $E(z)$ and $H(z)$ by extrapolating in (25):

$$E_{+}(z) = \frac{1}{2}[E(z) + \eta H(z)]$$
$$E_{-}(z) = \frac{1}{2}[E(z) - \eta H(z)] \tag{26}$$

From this, two valuable quantities can be defined: the wave impedance and the reflection coefficient.

$$Z(z) = \frac{E(z)}{H(z)}, \qquad (wave\ impedance) \tag{27}$$

$$\Gamma(z) = \frac{E_{-}(z)}{E_{+}(z)}, \qquad (reflection\ coefficient) \tag{28}$$

The most simple form of reflection and transmission comes from a planar interface dividing two dielectric and/or conducting material with characteristic impedances η, η', as in Figure 1.

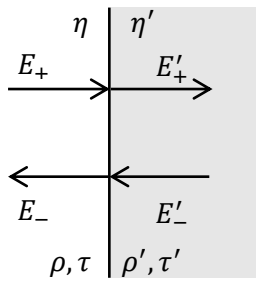

Figure 1: A field propagating forward and backward through an interface.

The elementary reflection (ρ) and transmission (τ) coefficients (also known as Fresnel coefficients) are defined as:

$$\rho = \frac{\eta' - \eta}{\eta' + \eta} = \frac{n - n'}{n + n'} \tag{29}$$

$$\tau = \frac{2\eta'}{\eta' + \eta} = \frac{2n}{n + n'} \tag{30}$$

where the last equal sign is derived from (6). Since the field is normally incident the electric and magnetic field on one side of the interface must equal the electric and magnetic field on the other side.

$$\begin{aligned} E_+ + E_- &= E'_+ + E'_- \\ \frac{1}{\eta}(E_+ - E_-) &= \frac{1}{\eta'}(E'_+ - E'_-) \end{aligned} \tag{31}$$

The equations in (31) can be rewritten in matrix form as:

$$\begin{bmatrix} E_+ \\ E_- \end{bmatrix} = \frac{1}{\tau}\begin{bmatrix} 1 & \rho \\ \rho & 1 \end{bmatrix}\begin{bmatrix} E'_+ \\ E'_- \end{bmatrix} \tag{32}$$

Using (28) together with (32) and the fact that $\tau = 1 + \rho$ yields:

$$\Gamma = \frac{E_-}{E_+} = \frac{\frac{1}{\tau}(\rho E'_+ + E'_-)}{\frac{1}{\tau}(E'_+ + \rho E'_-)} = \frac{\rho + \frac{E'_-}{E'_+}}{1 + \rho\frac{E'_-}{E'_+}} = \frac{\rho + \Gamma'}{1 + \rho\Gamma'} \tag{33}$$

for the reflection coefficient from a single interface. One could also look at the total transmission, defining it as what comes out from the interface divided by what goes in:

$$T = \frac{E'_+}{E_+} = \frac{E'_+}{\frac{1}{\tau}(E'_+ + \rho E'_-)} = \frac{(1+\rho)E'_+}{(1 + \rho\frac{E'_-}{E'_+})E'_+} = \frac{1+\rho}{1+\rho\Gamma'} \tag{34}$$

In our measurements, there will (theoretically) only be an incident wave from the left in Figure 1, so that $E'_- = 0$. This simplifies (33) and (34) as $\Gamma' = E'_-/E'_+ = 0$ to:

$$\Gamma = \rho \tag{35}$$

$$T = 1 + \rho \tag{36}$$

As we can see, for a single interface the reflection and transmission is easily calculated.

2.2.2 One-layer structure

The second most simple kind of interface is that of a single dielectric slab, see Figure 2. In this figure we see a two-interface slab with characteristic impedance η_1 separated by the two mediums η_x and η_y.

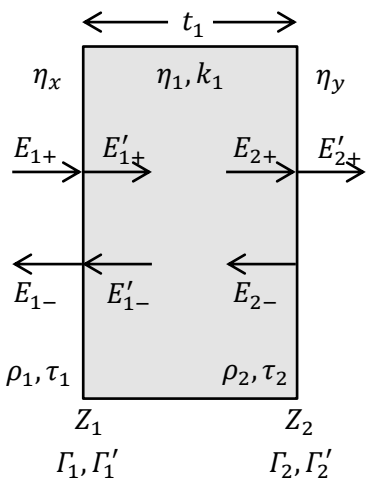

Figure 2: A single dielectric one-layer slab.

The thickness of the slab is t_1 and the wavenumber is $k_1 = \omega/c_1$, where c_1 is the speed of light in the material. The electromagnetic wave is set to be incident from the left and therefore there is only a forward wave in the medium η_y.

Using the same matrix notation as in the previous section (32) gives:

$$\begin{bmatrix} E_{1+} \\ E_{1-} \end{bmatrix} = \frac{1}{\tau_1}\begin{bmatrix} 1 & \rho_1 \\ \rho_1 & 1 \end{bmatrix}\begin{bmatrix} E'_{1+} \\ E'_{1-} \end{bmatrix} = \frac{1}{\tau_1}\begin{bmatrix} 1 & \rho_1 \\ \rho_1 & 1 \end{bmatrix}\begin{bmatrix} e^{jk_1t_1} & 1 \\ 1 & e^{-jk_1t_1} \end{bmatrix}\begin{bmatrix} E_{2+} \\ E_{2-} \end{bmatrix}$$
$$= \frac{1}{\tau_1}\begin{bmatrix} 1 & \rho_1 \\ \rho_1 & 1 \end{bmatrix}\begin{bmatrix} e^{jk_1t_1} & 1 \\ 1 & e^{-jk_1t_1} \end{bmatrix}\frac{1}{\tau_2}\begin{bmatrix} 1 & \rho_2 \\ \rho_2 & 1 \end{bmatrix}\begin{bmatrix} E'_{2+} \\ 0 \end{bmatrix} \quad (37)$$

Performing the matrix multiplications yields

$$E_{1+} = \frac{e^{jk_1t_1}}{\tau_1\tau_2}(1 + \rho_1\rho_2 e^{-2jk_1t_1})E'_{2+} \quad (38)$$

$$E_{1-} = \frac{e^{jk_1t_1}}{\tau_1\tau_2}(\rho_1 + \rho_2 e^{-2jk_1t_1})E'_{2+} \quad (39)$$

for the incoming and outgoing fields. With this information we can calculate the reflection and transmission signal, as in the previous section:

$$\Gamma_1 = \frac{E_{1-}}{E_{1+}} = \frac{\rho_1 + \rho_2 e^{-2jk_1t_1}}{1 + \rho_1\rho_2 e^{-2jk_1t_1}} = \frac{\rho_1 + \Gamma_2 e^{-2jk_1t_1}}{1 + \rho_1\Gamma_2 e^{-2jk_1t_1}} \quad (40)$$

$$T = \frac{E'_{2+}}{E_{1+}} = \frac{\tau_1\tau_2 e^{-jk_1t_1}}{1 + \rho_1\rho_2 e^{-2jk_1t_1}} \quad (41)$$

Since there is no field going to the left in media η_b, the reflection from the second interface is $\Gamma_2 = \rho_2$, as derived in previous section. The transmission has a delay factor of $e^{-jk_1t_1} = e^{-j\omega T/2}$, which represents the direct-way travel time delay through the slab. The reflection is instead composed of two parts, one from the first interface and another (two-way travel delayed) from the second.

2.2.3 Multilayer structure

Moving on to the more general case of an M-layer structure, as seen in Figure 3, we finalize our theory for reflection and transmission.

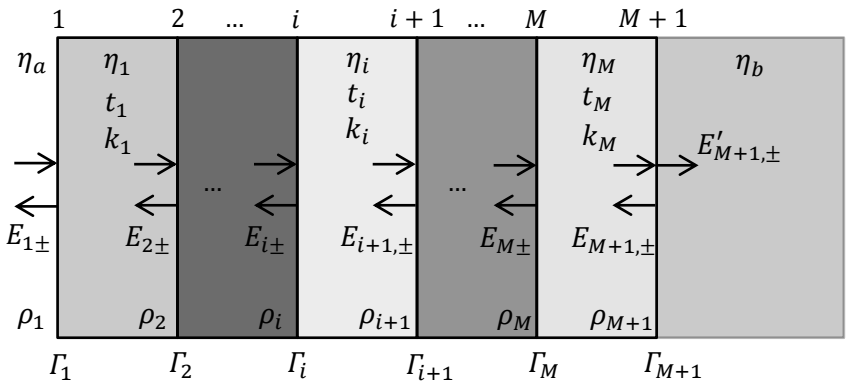

Figure 3: A multilayer structure

In this figure there are M slabs and $M+1$ interfaces, and together with the left and right media, $M+2$ dielectrics. The entire reflection response $\Gamma_1 = E_{1-}/E_{1+}$ is obtained recursively by matrix multiplications (as done in the previous section). The reflection coefficients ρ_i are defined as before, in terms of characteristic impedances or refractive indices:

$$\rho_i = \frac{\eta_i - \eta_{i-1}}{\eta_i + \eta_{i-1}} = \frac{n_{i-1} - n_i}{n_{i-1} + n_i}, \qquad i = 1, 2 \dots, M+1 \tag{42}$$

In (43) the forward/backwards fields at the left of interface i are related to those at the right.

$$\begin{bmatrix} E_{i+} \\ E_{i-} \end{bmatrix} = \frac{1}{\tau_i} \begin{bmatrix} e^{jk_i t_i} & \rho_i e^{-jk_i t_i} \\ \rho_i e^{jk_i t_i} & e^{-jk_i t_i} \end{bmatrix} \begin{bmatrix} E_{i+1,+} \\ E_{i+1,-} \end{bmatrix}, \qquad i = M, M-1, \dots, 1 \tag{43}$$

From this, the reflection and transmission response can be calculated:

$$\Gamma_i = \frac{\rho_i + \Gamma_{i+1} e^{-2jk_i t_i}}{1 + \rho_i \Gamma_{i+1} e^{-2jk_i t_i}}, \qquad i = M, M-1, \dots, 1 \tag{44}$$

$$T_i = \frac{\tau_i T_{i+1} e^{-jk_i t_i}}{1 + \rho_i \Gamma_{i+1} e^{-2jk_i t_i}}, \qquad i = M, M-1, \dots, 1 \tag{45}$$

These equations can be implemented in simulations to handle any M-layer structure with each layer having different thicknesses, permittivity and conductivity.

One phenomenon that can occur for one-layer structures or higher is destructive and constructive interference of the reflected or transmitted wave. In (44) and (45) this would correspond to the numerator approaching zero for destructive interference and the denominator approaching zero for constructive interference. For reflection the destructive interference occurs when the wave reflected from the first interface is out of phase from the wave reflected at the second interface. For the one-layer case in Figure 2 this happens when the thickness t_1 is half a wavelength or multiples thereof, $n\lambda/2$.

Let's assume the thickness t_1 is $300\ \mu m$ and we want to calculate the permittivity the material must have to correspond to the $\lambda/2$ situation. From (5) and (7) we get:

$$300\ \mu m = \frac{\lambda}{2} = \frac{c}{2f} = \frac{c_0}{2fn} = \frac{c_0}{2f\sqrt{\varepsilon}} \leftrightarrow \varepsilon = \left(\frac{c_0}{2f \cdot 300 \cdot 10^{-6}}\right)^2 \tag{46}$$

from which the permittivity can be extracted.

2.3 Simulation Pre-study & Design plots

This subsection uses the theory derived above to simulate transmission and reflection for different material parameters. This gave a good foundation for deciding what materials would be interesting to measure upon (where one would get the most data from) as well as deciding what thickness the material should be and at what frequency the measurement should be performed for optimal data extraction. All of the graphs in this section are simulated at 60 GHz operating frequency, unless mentioned otherwise.

2.3.1 One-layer structure

Starting with a single-layer structure, the reflection and transmission was simulated. It was simulated by letting an electromagnetic wave travel through vacuum toward a substrate, as in Figure 4.

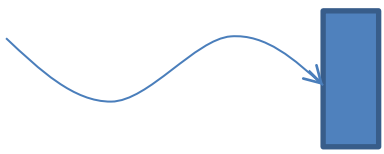

Figure 4: A uniform planar electromagnetic wave impinges upon a one-layer substrate.

The following figures display expected transmission and reflection when sweeping over different material parameters, such as conductivity, permittivity and thickness of the substrate. By looking at each variable separately, the action of each material parameter on its own will be clarified. In Figure 5 three graphs are plotted: the reflection when varying a material's conductivity, the reflection vs. the thickness of the substrate and finally the reflection vs. permittivity.

In Figure 5a and Figure 5c the thickness of the substrate is 300 µm. In Figure 5b the conductivity is $\sigma = 4.1 \cdot 10^7\ S/m$ which is equivalent to gold's conductivity at room temperature [10]. The real part of the permittivity is held constant at 1 in both Figure 5a and Figure 5b. For Figure 5c the conductivity is set to zero.

As (40) and (21) predicts, the reflection in Figure 5a increases linearly in the dB-scale as the conductivity increases, until it starts to approach 0 dB asymptotically.

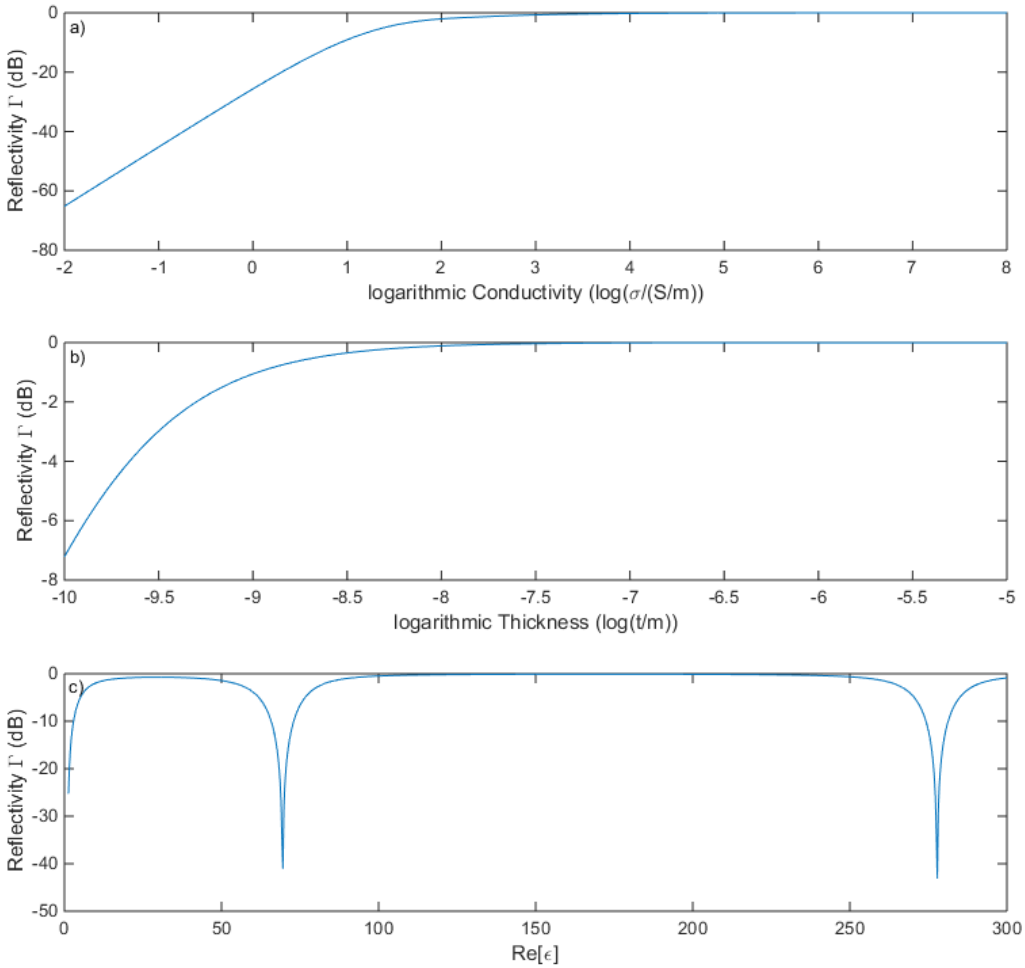

Figure 5: Plot a) The reflection of a 300 µm one-layer slab over varying conductivities. The real part of the permittivity is 1, representing a metal.

Plot b) The reflection from a one-layer slab with varying thickness. The conductivity used in this simulation corresponds approximately to that of gold at room temperature. The thickness range is from 0.1 nm to 10 µm. The real part of the permittivity is 1.

Plot c) The reflection vs. permittivity of a 300 µm slab. The occurrence of the repetitive destructive half-wavelength interference is visible. The conductivity is set to zero.

From Figure 5b one observes a similar appearance; the reflection increases asymptotically towards 0 dB as the thickness of the substrate is increased. This is also consistent with (40). If the conductivity of the substrate is high, the reflection will approach full reflection at a certain thickness. This is related to the skin depth of a material, expressed as $\delta = \sqrt{2/\omega\mu\sigma}$, which is a figure of merit for the power attenuation a field experiences traveling through a material. If the conductivity, permeability or frequency increases, the skin depth would decrease, resulting in a higher reflection (lower transmission) [11].

In Figure 5c a difference in appearance is noticed, as the reflection drastically decreases at certain permittivity values. This corresponds to the half-wavelength destructive interference. It is also worth noting that "metals" of such low conductivities as simulated here do not exist to any known extent. The materials with such low conductivity would instead have a real permittivity higher than 1, which would increase the reflection from the material [12].

By combining the variation of conductivity and thickness into a colormap showing the reflection and the transmission, one acquires Figure 6. The color scale is the reflection in dB and the real part of the permittivity is 1. The region where the reflection magnitude has a significant gradient is the most promising area to measure upon, since one would see a distinct difference in reflection when varying conductivity or thickness of the substrate.

Figure 6 also plots the corresponding colormap for transmission. Its gradient is located approximately 2 orders of magnitude higher in conductivity, pointing in favor for measuring materials with higher conductivities in transmission. Preferable one would like to obtain both reflection and transmission data since this maximizes the parameter range where material characterization is possible.

Figure 7 maps the reflection and transmission when sweeping over the material's real permittivity and conductivity. The thickness is set to 300 µm, since this was approximately the same thickness as our silicon wafers had during measurement. It appears that above a certain conductivity ($\sim 10^2\ S/m$) the effect of the permittivity no longer alters the reflection, but for low conductivities the periodicity from the permittivity that was seen in Figure 5c is present. A line for possible silicon (Si) substrate conductivities is included, showing what kind of reflection and transmission one would expect from this substrate [13].

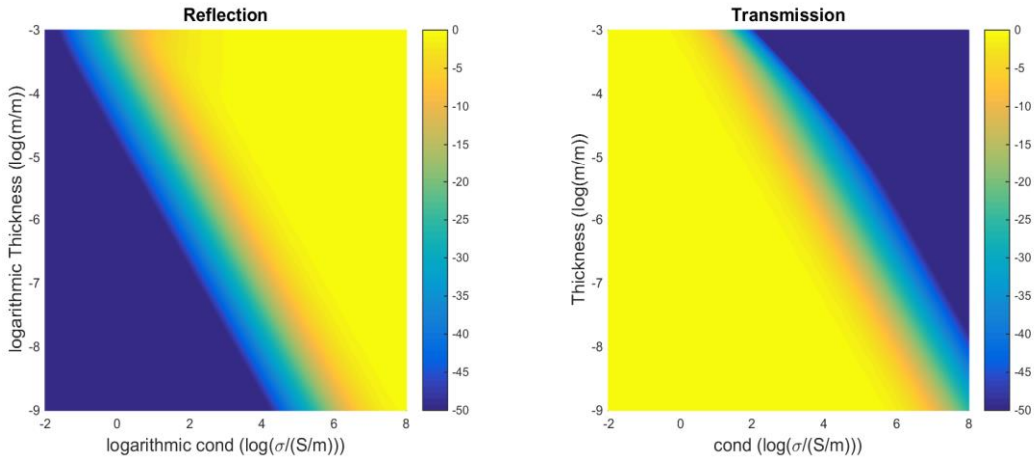

Figure 6: Reflection and Transmission (respectively) vs. thickness and conductivity for a single-layer slab. The real part of the permittivity is 1.

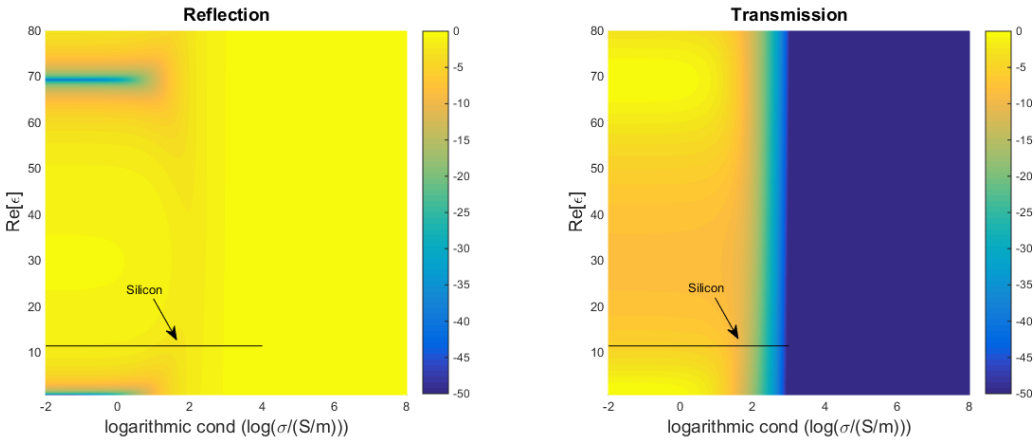

Figure 7: Reflection and Transmission (respectively) vs. real permittivity and conductivity for a single-layer slab. The thickness of the slab is set to 300 µm.

2.3.2 Multilayer structure

Figure 8 depicts a two-layer structure, representing a thin film on a thicker substrate. The abbreviation PEDOT:PSS used in this section stands for poly(3,4-ethylenedioxythiophene) polystyrene sulfonate and is a conductive polymer which can be used for thin films.

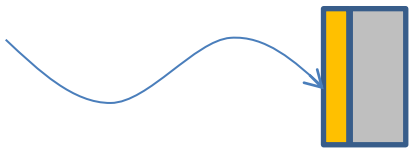

Figure 8: An electromagnetic wave impinges upon a two-layer slab.

In these simulations the substrate is silicon (Si) and the thin film's parameters are swept. The silicon is modeled to have a conductivity of $\sigma = 1.6 \cdot 10^{-3}\ S/m$ and a real permittivity of $Re[\varepsilon] = 11.68$ [10] [13]. Figure 9 maps the reflection and transmission as the conductivity and the thickness of the thin film varies. The change in reflection is not as profound (mind the scale of the colorbar) as in the figures above, since the silicon substrate's variables are constant. The consequence of this is that the structure will always have a certain minimum reflection, which will be much higher than in the one-layer case.

A very low transmission is observed when the thin film is highly conductive ($> 10^7\ S/m$), for example gold (Au), titanium (Ti) and possible PEDOT:PSS thin films are marked in the Figure 9 [10] [14] [15]. The gold shows a very high reflection for most thicknesses and it's not until very very thin (1-10 nm) films are applied that one starts to see some measurable transmission. The titanium should be very interesting to measure upon since it spans the gradient part of the colormap very well. Unfortunately it seems that the PEDOT:PSS possibilities are a bit too low in conductivities to really gain much information from such a sample.

In Figure 10 the permittivity and conductivity of the thin film are swept. The dependence of the permittivity is not as apparent as in Figure 7. This is mostly because the thin film is considerable thinner than the one-layer slab case.

In Figure 11 the substrate thickness vs. the thin film conductivity is swept. One can observe that the two-layer slab will give a minimum reflection at certain substrate thicknesses; this corresponds to the $\lambda/2$ thickness explained in (46).

For real measurements it becomes impractical having to fit the substrate thickness to minimize its reflection. Luckily when one does measurements, the frequency is usually not fixed to a specific value. Therefore, as the frequency is swept during measurements, one will hopefully cross the minimum values of substrate reflection and be able to maximize the relative response from the thin film sample.

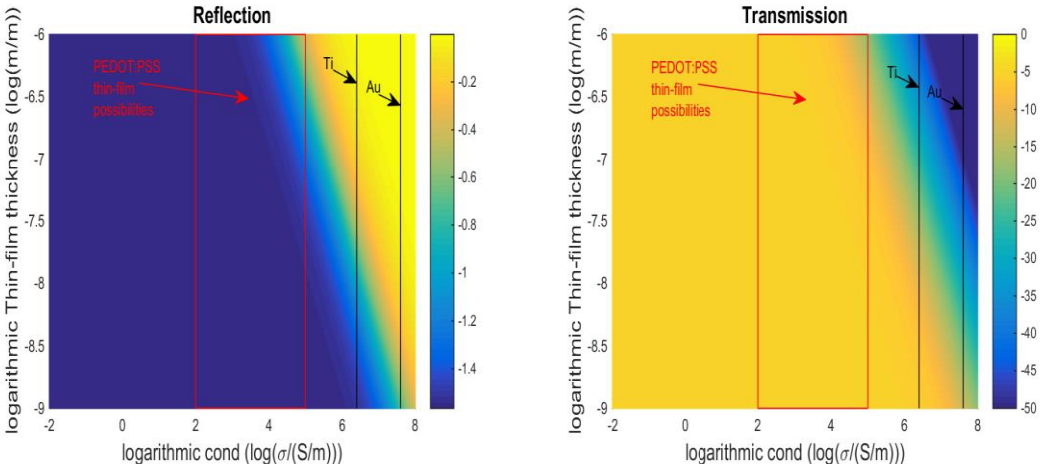

Figure 9: Reflection and transmission vs. thickness and conductivity of thin film. The substrate is 300 µm and the thin film has a real permittivity of 1.

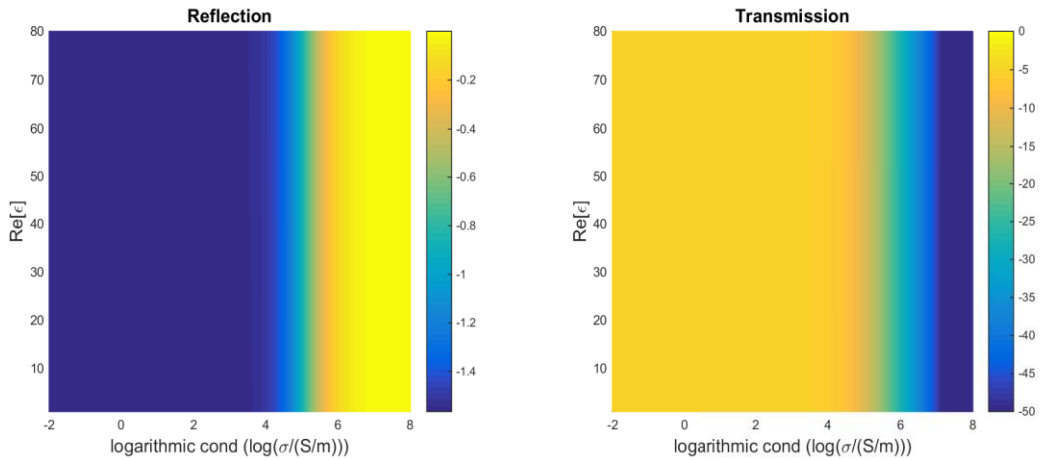

Figure 10: Reflection and transmission vs. real permittivity and conductivity of thin film. The substrate is 300 µm and the thin film is 300 nm.

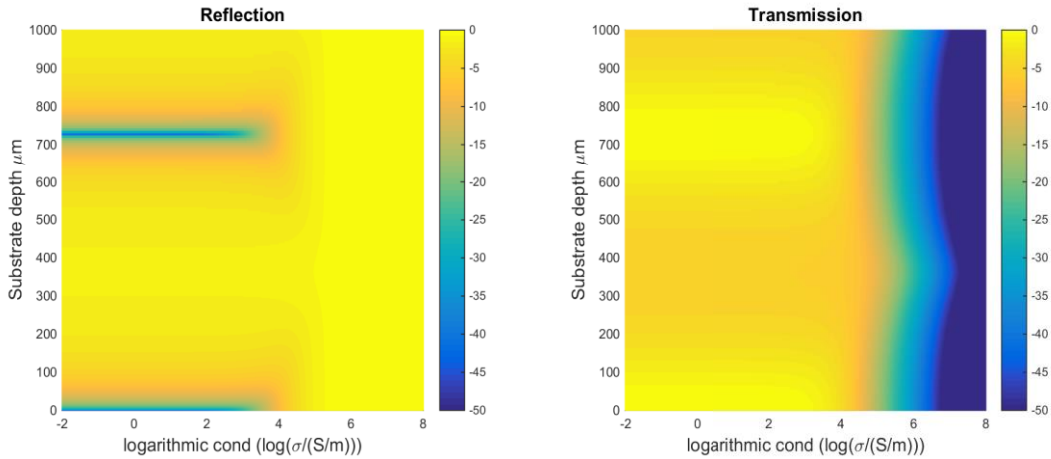

Figure 11: Reflection and transmission vs. substrate thickness and conductivity of thin film. The thin film is 300 nm and its real permittivity is 1.

Table 1 on the next page shows the 4 samples chosen to be measured and simulated. The two dielectrics were made from PMMA. PMMA stands for Poly(Methyl MethAcrylate) and is a thermoplastic polymer, also known under one of its trade names; Plexiglas. They were chosen because reference measurements on these samples from the institution existed. The two conductors chosen were: a single-layer slab of silicon and a two-layer slab of thin gold film on silicon. Table 1 also discloses all the constant material parameters used for the simulations. Figure 12 shows a picture of the samples.

Sample	Assumed value
PMMA sheet	
t_1	2.095 cm
$Im[\varepsilon]$	$0.009i$ [16]
PMMA container	
t_1	2.09 cm
t_2	0.51 cm
t_3	2.05 cm
$Im[\varepsilon]$	$0.009i$
Si wafer	
t_1	300 μm
$Re[\varepsilon]$	11.68 [13]
Gold film on Si	
t_1	10 nm
$Re[\varepsilon]_1$	1
t_2	$350 + 20$ μm
$Re[\varepsilon]_2$	11.68
ρ_2	20 $k\Omega cm$

Table 1: Assumed values for the different samples.

CHAPTER 3

3 Methodology

The two different measurement setups are examined and how the measurements were performed is explained. The necessary processing steps for matching simulated to measured data is covered and the method used for extracting parameters is shown.

3.1 Measurements

Figure 12 shows a picture of the measurement samples focused on in this report. From left to right: A PMMA sheet, a PMMA container (small air gap between two PMMA sheets) and wafers, such as low resistivity silicon and a thin gold film on silicon.

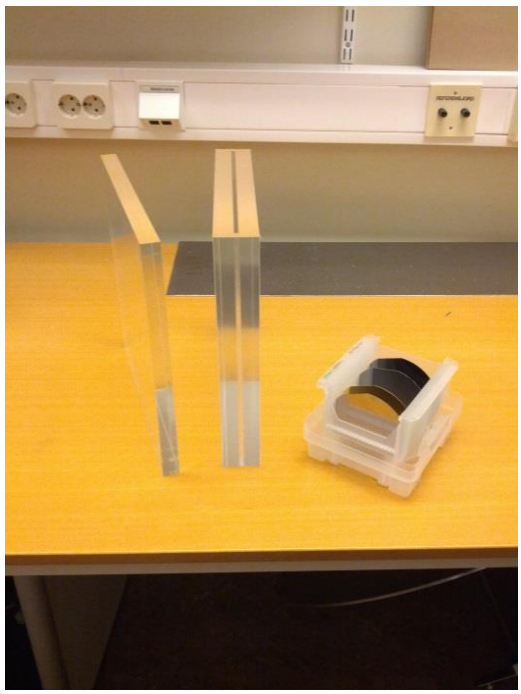

Figure 12: From the left to the right: PMMA sheet, PMMA container and different wafers.

Measurements were performed in both time- and frequency domain. A VNA (Vector Network Analyzer, Agilent Technologies E8361A) was used for the frequency-domain while a sampling oscilloscope (Agilent Technologies 86100D) together with a sampling module (Agilent Technologies 86118A) and an in-house wavelet generator was used for the time-domain. Figure 13 and Figure 14 depicts a crude schematic for the transmission and reflection measurement setups. In time domain measurements the signal is created by a short pulse, which is equivalent to a broadband signal. Therefore many frequencies are present at the same time, enabling time resolved measurements to be possible. In frequency domain the VNA measures the reflected and transmitted scattering parameters in a narrowband frequency signal, the frequency is then changed and the process repeated.

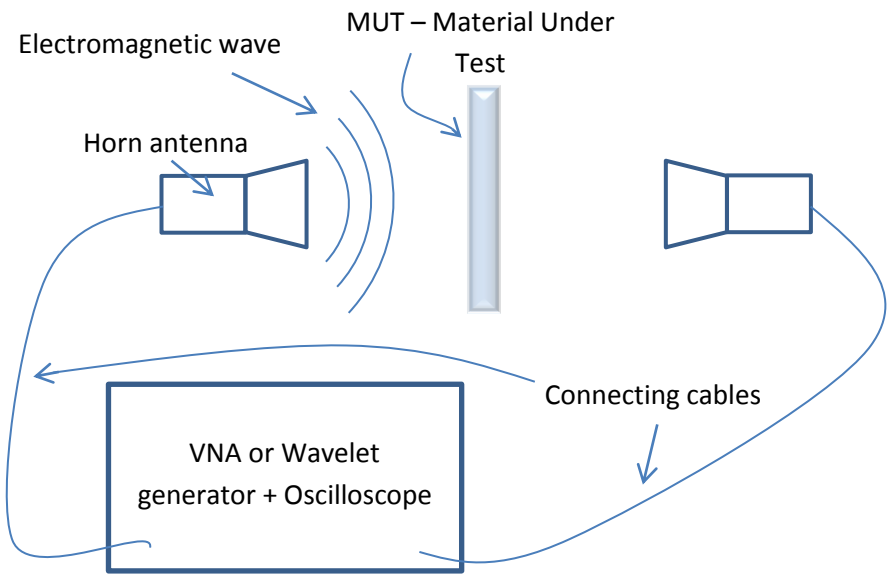

Figure 13: A schematic of transmission measurements.

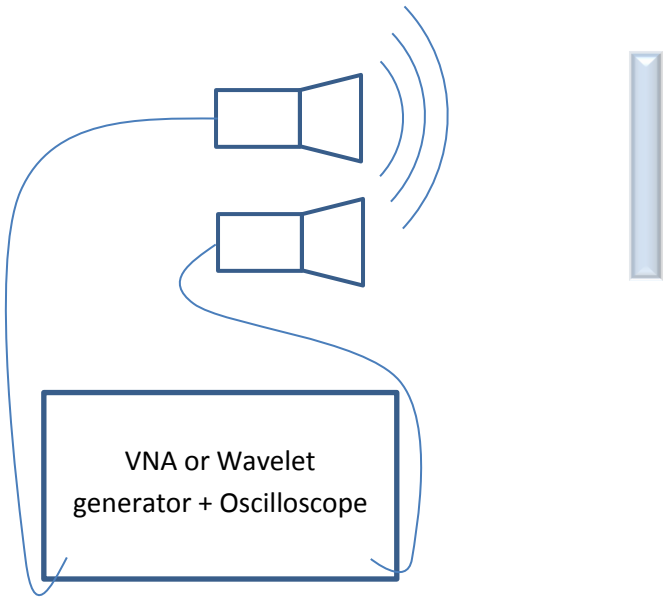

Figure 14: A schematic of reflection measurements.

3.3.1 Frequency domain

Frequency domain measurements were done for both reflection and transmission, using lens and horn antennas. The antennas were connected to cables via waveguide adapters and free space measurements were performed. The reference for the reflection setup was a copper-plate and in later measurements a thick gold film on silicon, as this material theoretically should have the highest possible reflection (of what can be produced in-house in our labs), as we can see in Figure 9. One problem that later arose when examining some data was that the reference object had not been placed at exactly the same distance as the samples being investigated.

A reflection measurement setup can be seen in Figure 15. In this figure the thick gold film on silicon is seen. In these measurements the aperture for holding the wafers consisted of a hole in an absorber sheet, whereupon the wafer was placed.

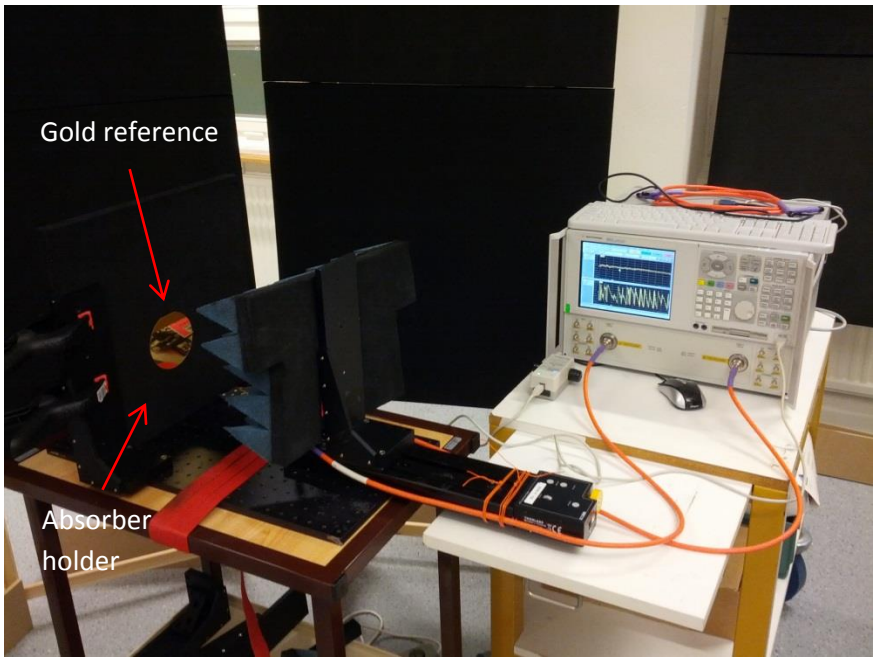

Figure 15: Reflection setup from the final round of measurements. A thick gold film on an Si-wafer is seen in the picture, this served as the normalization reference.

3.3.2 Time domain

Both reflection and transmission measurements were performed in time domain as well. A transmission measurement setup can be seen in Figure 16. The lens antennas were used in this case.

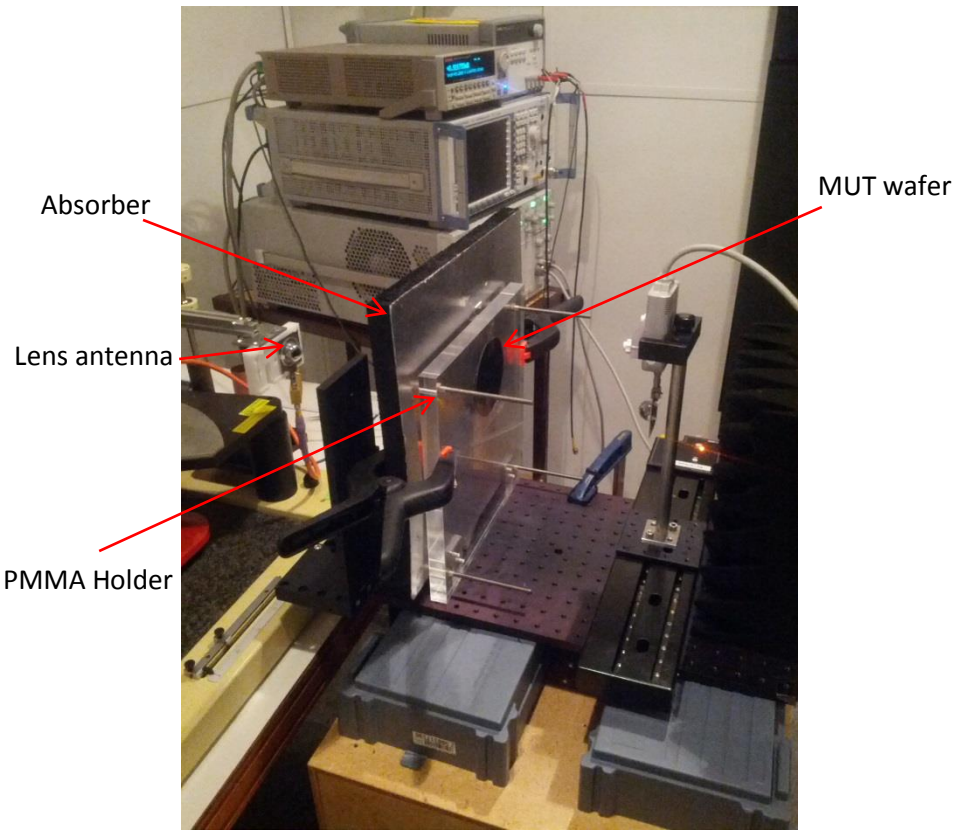

Figure 16: Transmission setup in time-domain.

In this setup another kind of holder aperture for the wafers was used. It consisted of a PMMA sheet and an absorber with a hole. The wafer was placed on the back of the PMMA sheet. The problem with this method is that when you remove the wafer and place another it is hard to make certain that it arrives in the exact same spot. It also introduces more things to simulate and measure since the PMMA sheet has to be incorporated into the simulations.

3.2 Signal Processing

To be able to compare the measured data to the simulated, post measurement processing was necessary. Since no calibration kit for the waveguide adapter existed (we could only calibrate to the cable tip), we used a method where the data was normalized to a reference sample. For reflection this means that the reference object would be something with a very high reflection at all frequencies, for example a thick metal sheet. For transmission this reference would correspond to open transmission without anything in the pathway.

After this was done, one had to remove multiple reflections from the data to get the wanted signal. Figure 17 shows a signal processing flow-chart, representing the necessary steps which had to be performed before the simulated data could be compared to the measured. If the data came from time domain (with the in-house wavelet generator) one had to transform to frequency domain before normalization was performed. If the data was obtained in frequency domain, normalization could be performed immediately. Therefore it does not matter whether the data was obtained from frequency or time domain.

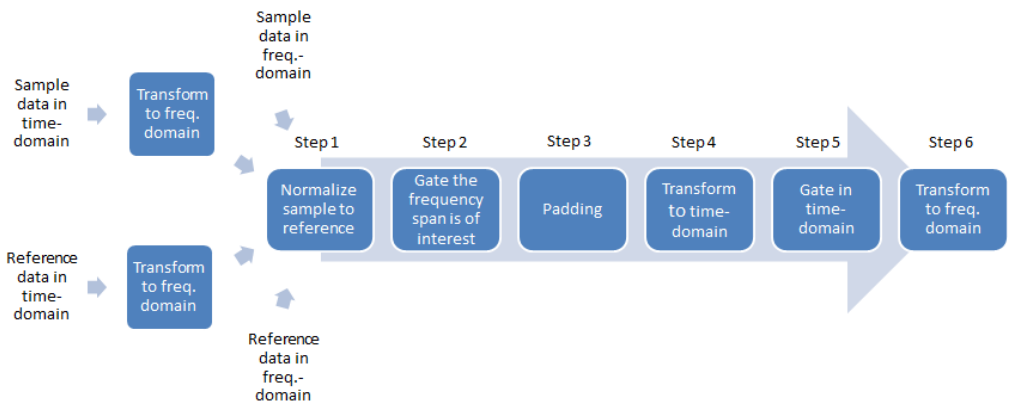

Figure 17: Signal processing flow-chart.

The six steps outlined in the figure are:

1, *Normalization of the sample to reference.* This was used to overcome the fact that we did not have calibration kit for the antenna. Any misalignment or angle error in both the sample and reference would also be managed with this method.

2, *Gate the frequency span of interest.* In our case this corresponded to 40-60 GHz.

3, *Padding.* A mathematical trick used to fill the data vector with equally stepped zeros from 40 GHz down to 0 GHz to mitigate gating artifacts.

4, *Transform to time domain.*

5, *Gate in time-domain.* This was done to remove multiple reflections from the measured data and, in some cases, internal antenna reflections.

6, *Transform to frequency domain.* The processing steps completed. The data could now be compared to simulated data, which had undergone the same processing steps.

Figure 18 and Figure 19 shows two plots in step 5, where gating is performed in time domain. Figure 18 is from a reflection measurement of a PMMA container and Figure 19 from a transmission measurement of a gold film on a silicon substrate.

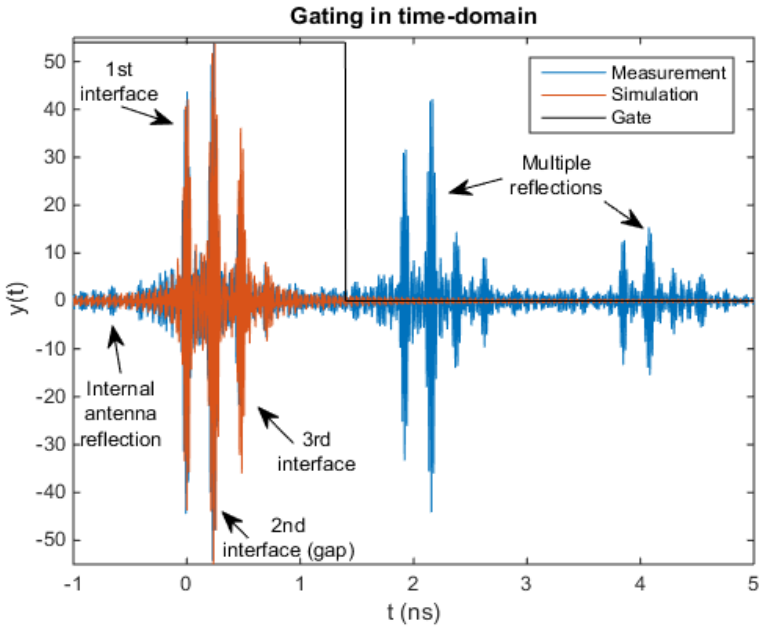

Figure 18: Time domain signal of reflection from a PMMA container, notice the internal antenna reflection at the start of the signal, as well as the multiple reflections after the first reflection.

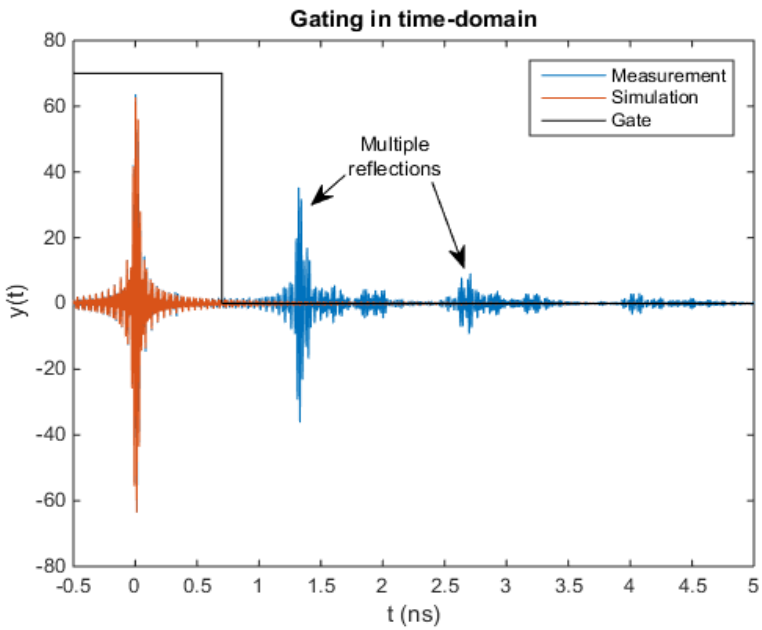

Figure 19: Time domain signal of transmission from a thin gold film on silicon. Notice the multiple reflections.

3.3 Parameter extraction

By simulating the measurement setup as close to reality as possible, the simulated data can be compared to the measured data and a parameter extraction is possible.

Figure 20 shows the simulated reflection with added thermal noise of a two-layer slab: a thin gold film on a silicon wafer. The gold layer was 5 nm thick and had a conductivity of $\sigma = 4.1 \cdot 10^7\ S/m$ [10]. The silicon substrate was 300 µm thick and had a permittivity of $Re[\varepsilon] = 11.68$ and conductivity $\sigma = 1.6 \cdot 10^{-3}\ S/m$ [10] [13].

The complex noise added in Figure 20 is Gaussian noise, which amplitude is calculated according to $\sqrt{N_{th}} = \sqrt{kT \cdot BW}$, where k is Boltzmann's constant, T is the absolute temperature in kelvins and BW the bandwidth of the measurement (in this case 10 kHz) [17]. The noise is added as $\Gamma = E_- + \boldsymbol{e_1}/E_+ + \boldsymbol{e_2}$. The air gap in the simulation is added to mirror an actual setup as much as possible.

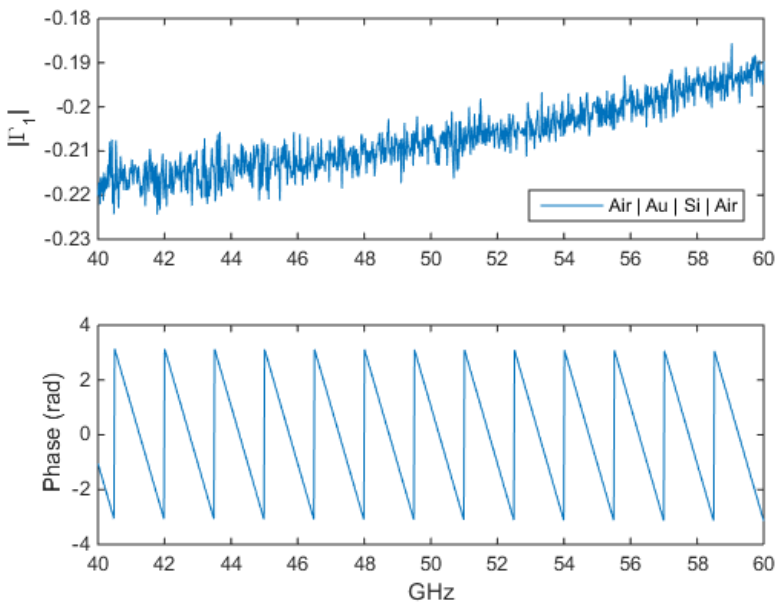

Figure 20: Simulated reflection from a two-layer sample (thin gold film on silicon) in dB with added thermal noise.

This “layer” will theoretically not change the amplitude of the wave in any way (in measurements it would however, due to spherical radiation properties of the antennas) but will alter its phase. That’s why it’s important to measure things exactly before executing real measurements.

The simulation with noise can then, for the sake of illustrating the method, be imagined to represent a real life measurement, Γ_{meas}. By comparing the measurement to many simulations with a varying material parameter, an error plot can be constructed: $Error = \sqrt{mean(|\Gamma_{meas} - \Gamma_{sim}|^2)}$. In Figure 21 such an error plot is shown when varying the thin film conductivity, assuming that all other parameters are known. Similar plots can be made to extract the permittivity or thickness of the material.

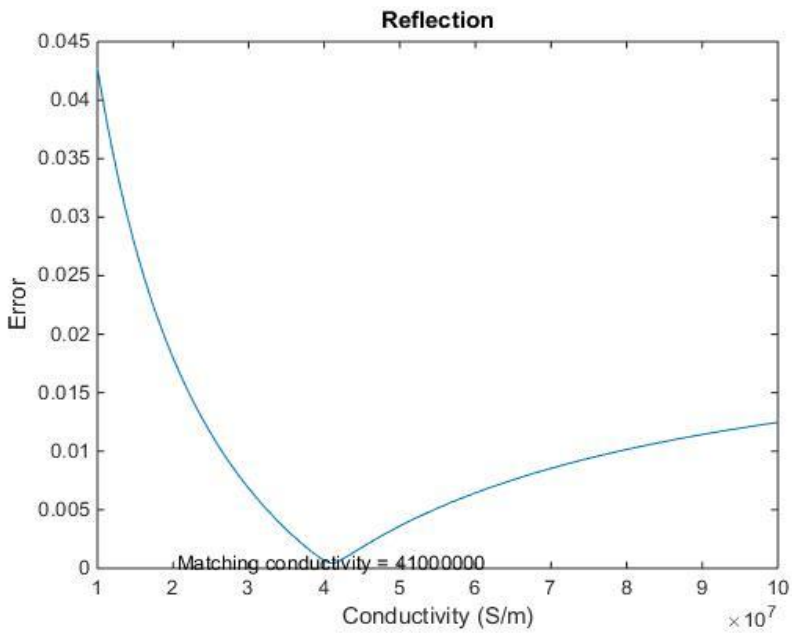

Figure 21: Error vs. Conductivity of the thin film. It finds the right value of $\sigma = 4.1 \cdot 10^7\ S/m$.

In some measurements a constant phase discrepancy was apparent, making the matching with simulations more difficult. This was induced because the distance from the antenna to the sample and the antenna to the reference sample differed slightly. When the normalization of the sample to the reference was

performed it therefore introduced a constant phase error. To be able to fit measurement and simulation in these cases, the gradient of the group delay (group delay being calculated as $\tau_g = -d\phi/d\omega$, where ϕ is the phase) and the magnitude of the signal were compared separately:

$$Phase\ error = W \cdot n \cdot \left| \left| \frac{d\tau_g}{df} \right|_{meas} - \left| \frac{d\tau_g}{df} \right|_{sim} \right|$$

$$Magnitude\ error = \left| |\Gamma_{meas}| - |\Gamma_{sim}| \right|$$

To make sure that the error from the magnitude and the error from the phase were at the same order of magnitude, a weighting factor W was added to the phase error. The size of this weighting factor was decided manually (to 10^{17}) by looking at the magnitude error and phase error, making sure they arrived at the same order of magnitude. A normalization vector n was also applied to the phase error. This was done because at reflection minima of the signal, the phase turned into large spikes which made the phase error vector useless. The normalization vector therefore consisted of disregarding the small areas of reflection minima. Finally the phase error and magnitude error were added together to get a pooled error and an error plot could be constructed.

One can also sweep more than one parameter at the same time, but this increases the amount of calculations exponentially. Preferably one should have very good guesses for most parameters and only one parameter being totally unknown. If this is not the case the calculations may take days and it might also find the "wrong" material parameters since if all parameters are chosen arbitrarily more than one possible solution exists. This can be seen by examining (44) and (45). The reflection and transmission coefficient in these two equations depend on the refractive index of the material, which in turn depend on the permittivity and permeability of the material (5). From (21) we know that by changing the real part of the permittivity or conductivity we change the effective permittivity. If one sweeps, for example, both thickness and conductivity over large spans the result could therefore be that it finds more than one match. For example, high conductivity thin film vs. lower conductivity thicker film.

CHAPTER 4

4 Results and discussion

4.1 PMMA sheet

The PMMA sheet on the left in Figure 12 was examined first. Figure 22 shows the fitting from reflection setups in frequency and time domain. The group-delay method, chapter 3, was used for this matching.

Looking at the legends in Figure 22, the measurements are the data obtained from the VNA or the sampling oscilloscope together with the in-house wavelet generator. The simulation is the matched signal that has undergone the same processing steps as the measured data. The ideal simulation is how the matched signal would look like without performing any signal processing. The material parameter fitted was the real part of the permittivity. In Figure 22 and Figure 23 one can see that the time and frequency domain signal is shifted compared to each other. This most likely happened because of an angle difference between the two setups (approximately 9°). The material parameter extracted for time domain was $Re[\varepsilon_r] = 2.38$ and for frequency domain $Re[\varepsilon_r] = 2.3$.

Figure 23 shows the results from transmission data in frequency and time domain. The magnitude match does not seem to be as good in this case; but this is most likely because the scale of the graph is different. It does, however, not appear to have the same angle problem as for the reflection setup since it finds almost the same value for both time and frequency domain matching. For time domain it extrapolates $Re[\varepsilon_r] = 2.5$ and for frequency domain $Re[\varepsilon_r] = 2.49$. This is $2.3\ \%$ lower than the expected value of $Re[\varepsilon_r] = 2.557$ [18].

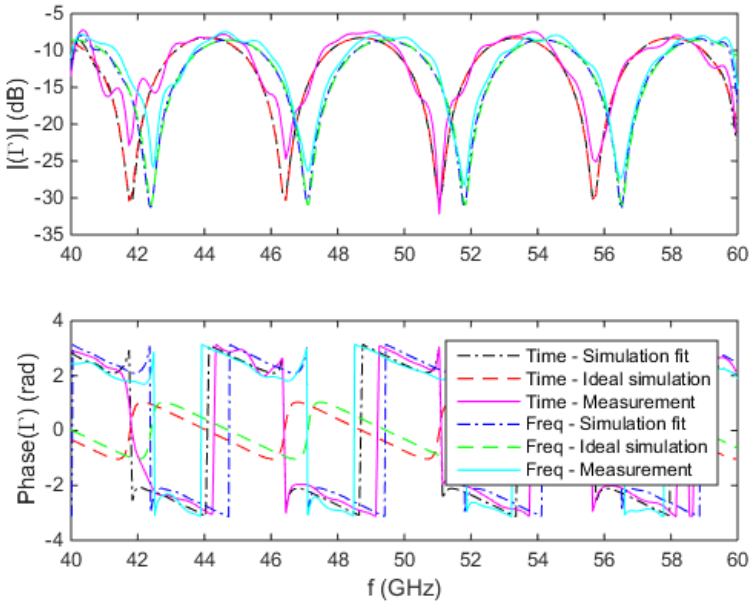

Figure 22: Time and frequency domain measurements of reflection from the PMMA sheet. The matched signal is shown in both ideal and processed state. The group-delay method of finding the material parameter was used for this case.

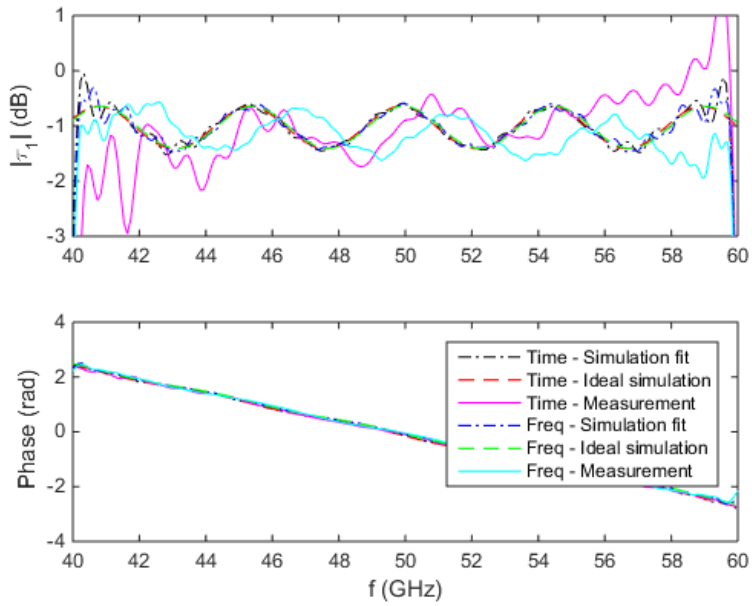

Figure 23: Time and frequency domain measurements of transmission from the PMMA sheet. The matched signal is shown in both ideal and processed state.

4.2 PMMA container

The PMMA container sample can be seen in the middle of Figure 12. Figure 24 shows the results from the reflection setups in frequency and time domain. The group-delay method was used in this matching. The simulated signals from both time and frequency domain looks very similar and this is also confirmed since it found very similar values for the real part of the permittivity. It also appears that an angle difference is still present, looking at the phase of the two measurement signals. The real part of the permittivity found was $Re[\varepsilon] = 2.56$ for time domain and $Re[\varepsilon] = 2.55$ for frequency domain. This is only $0.04\,\%$ lower than the expected value.

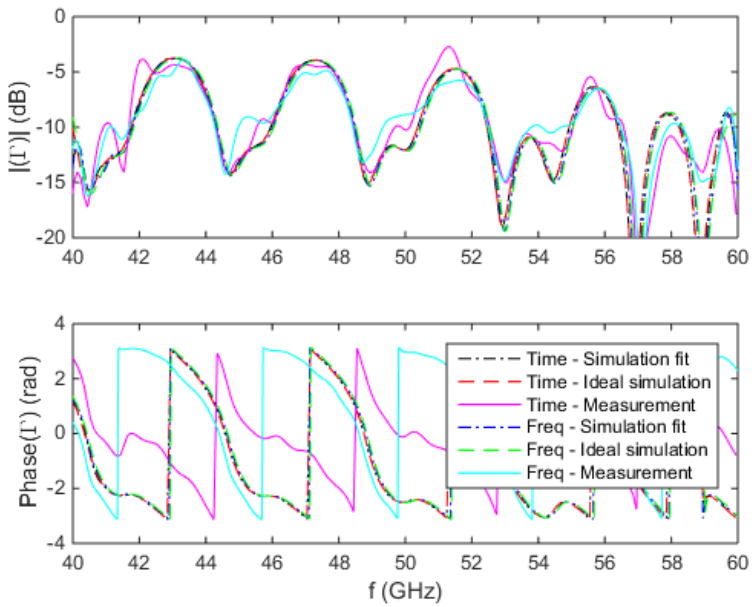

Figure 24: Time and frequency domain measurements of reflection from PMMA container. The matched signal is shown in both ideal and processed state. The group-delay method of finding the material parameter was used for this case.

Figure 25 shows the transmission data from frequency and time domain. The angle difference is present here as well (approximately 7°), looking at the phase. It also seems like the measured transmission is a bit lower than the simulated, even though the imaginary part of the permittivity is borrowed from an earlier PhD student's work with similar PMMA sheets [16]. The found values were $Re[\varepsilon_r] = 2.55$ for time domain and $Re[\varepsilon_r] = 2.58$ for frequency domain. This is ± 0.9 % off from the expected value.

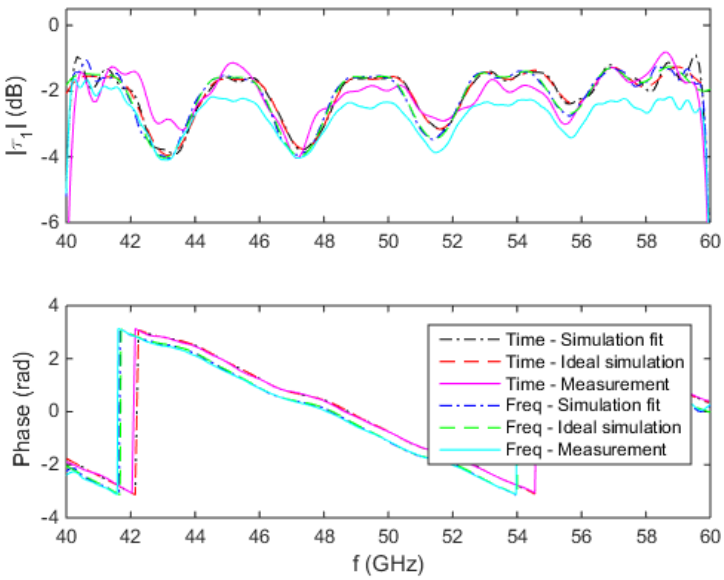

Figure 25: Time and frequency domain measurements of transmission from PMMA container. The matched signal is shown in both ideal and processed state.

The calculated percentage value off from the expected value of the permittivity is for those measurements only and there is no certainty that in repeating the measurements the same error would be found reliably.

4.3 Silicon wafer

The silicon wafer reflection results from frequency and time domain can be seen in Figure 26. The parameter fitted was the resistivity and in this case we had specifications from the manufacturer of what the resistivity of the silicon should be: $\rho = 4 - 7\ k\Omega cm$. That's why there are two additional lines in this plot that correspond to the expected appearance of the signal. The time domain lines are quite different from the frequency domain lines. This is because two different holders for attaching the wafers were used. In time domain a PMMA sheet was used to hold the wafer, this caused the pattern of large dips and tops that can be seen. For frequency domain a holder made from an absorbing aperture was used.

For the time domain measurement the expected signal seems to be a better fit than the simulation, but shifted in a similar way as the reflection case for the PMMA sheet, Figure 22. One possible explanation for the discrepancy of the fitted value and expected could therefore be that an angle difference was present between the sample and the reference. For the frequency domain measurement the expected value does not seem to fit since it has a higher

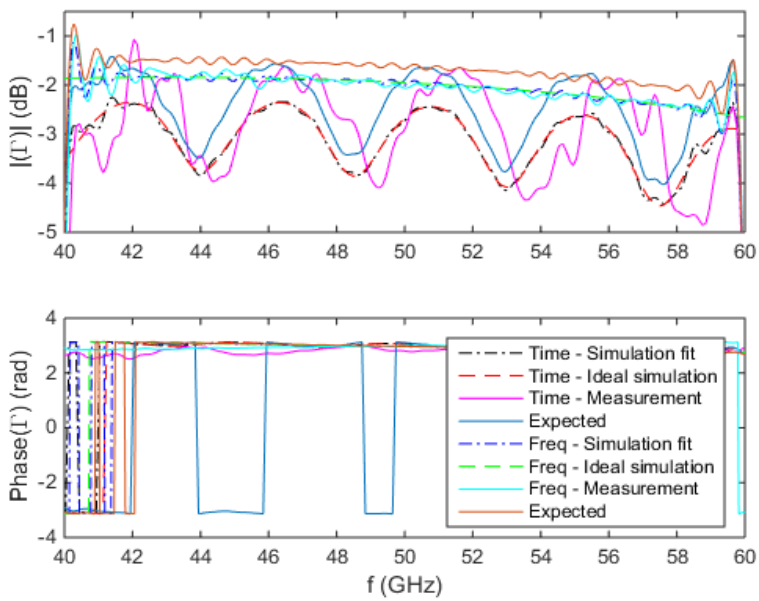

Figure 26: Time and frequency domain measurements of reflection from Si-wafer. The matched signal is shown in both ideal and processed state. The group-delay method of finding the material parameter was used.

reflection than the measured. The resistivity fitted was $\rho = 13.3\,\Omega cm$ for time domain and $\rho = 35.6\,\Omega cm$ for frequency domain, about 2 orders of magnitude off from the expected value.

Figure 27 shows the transmission result for the frequency and time domain. For the time domain it seems the expected value is a better fit once again, if accounted for an angle. The difference in frequency domain is however very small. The extrapolated values from time and frequency domain were still off by 2 orders of magnitude; $\rho = 9.9\,\Omega cm$ for time domain and $\rho = 101\,\Omega cm$ for frequency domain.

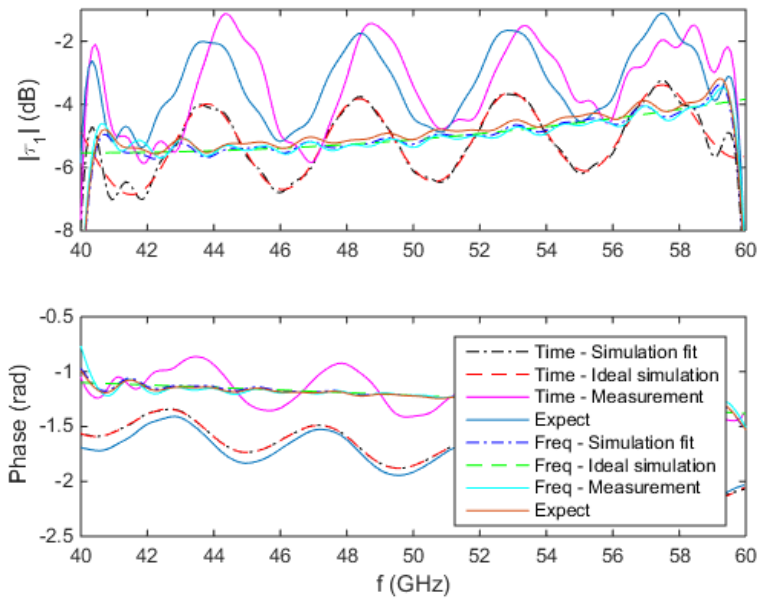

Figure 27: Time and frequency domain measurements of transmission from Si-wafer. The matched signal is shown in both ideal and processed state.

4.4 Thin gold film on silicon

The final sample was a thin gold film on a silicon substrate. Figure 28 shows the reflection results from frequency domain. Only frequency domain measurements were performed. The conductivity of the thin film was the material parameter fitted. As one can see from the figure, a very high reflection from the gold surface is present. The simulated fit found a value, $\sigma = 19.4\ MS/m$, approximately half of what it should be according to the expected value for bulk gold: $\sigma = 41.7\ MS/m$ [10]. This can be explained by the fact that thin sputtered films can have lower conductivities than in bulk form.

Figure 29 shows the transmission results from frequency domain. The phase match was originally not as good as shown here, what is shown here is instead what it would look like with an angle of 18° degrees away from normal incidence. The path traveled in the sample is therefore 20 µm longer than it should be. The value extrapolated, $\sigma = 12.3\ MS/m$, is on the same order of magnitude as in the reflection case.

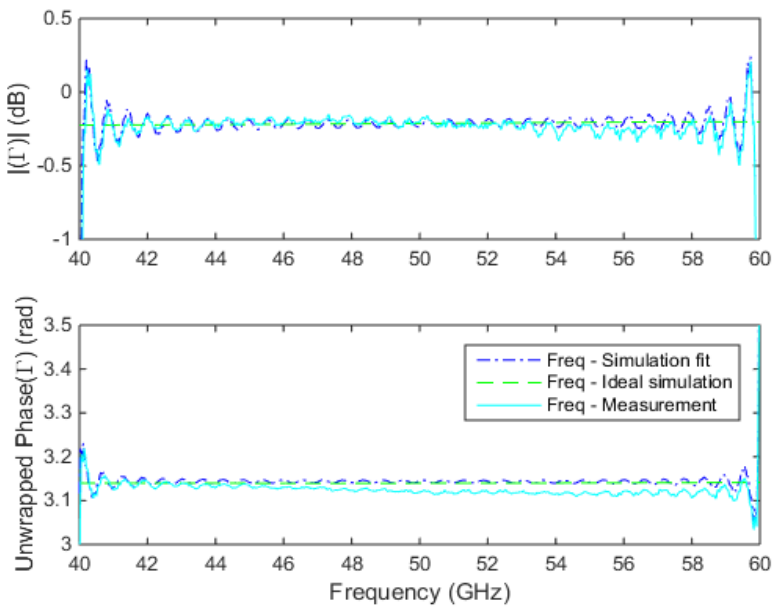

Figure 28: Frequency domain measurements of reflection from thin gold film on silicon substrate. The matched signal is shown in both ideal and processed state.

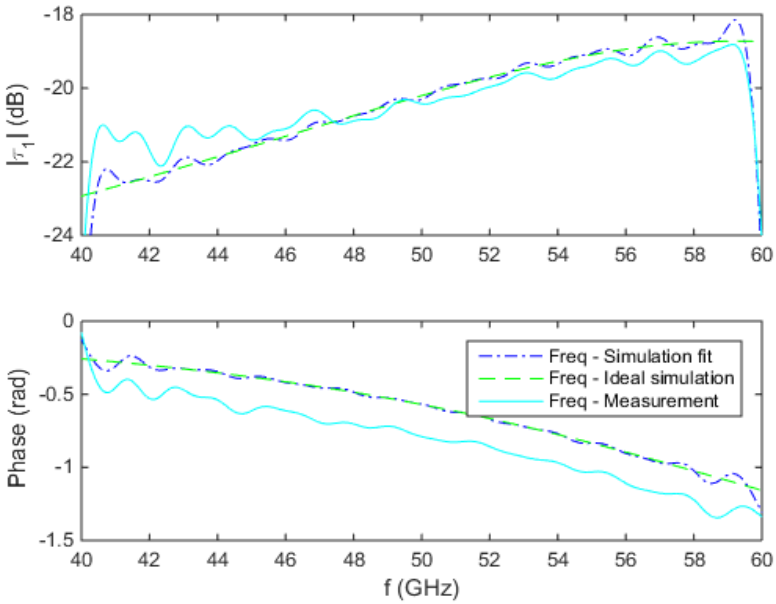

Figure 29: Frequency domain measurements of transmission from Si-wafer. The matched signal is shown in both ideal and processed state.

Table 2 on the next page summarizes the extrapolated and expected values for the different samples and the two measurement setups. In the appendix the source code for the design plots (section 2.3) can be seen in their generalized form.

Sample	Time domain	Frequency domain
PMMA sheet		
Reflection	$Re[\varepsilon] = 2.38$	$Re[\varepsilon] = 2.3$
Transmission	$Re[\varepsilon] = 2.5$	$Re[\varepsilon] = 2.5$
Expected	$Re[\varepsilon] = 2.557$ [18]	$Re[\varepsilon] = 2.557$
PMMA container		
Reflection	$Re[\varepsilon] = 2.56$	$Re[\varepsilon] = 2.55$
Transmission	$Re[\varepsilon] = 2.55$	$Re[\varepsilon] = 2.58$
Expected	$Re[\varepsilon] = 2.557$	$Re[\varepsilon] = 2.557$
Si wafer		
Reflection	$\rho = 13.3\ \Omega cm$	$\rho = 35.6\ \Omega cm$
Transmission	$\rho = 9.9\ \Omega cm$	$\rho = 101\ \Omega cm$
Expected	$\rho = 4 - 7\ k\Omega cm$	$\rho = 4 - 7\ k\Omega cm$
Gold film on Si		
Reflection	-	$\sigma = 19.4\ MS/m$
Transmission	-	$\sigma = 12.3\ MS/m$
Expected (Bulk)	-	$\sigma = 41.7\ MS/m$ [10]

Table 2: Fitted values from time and frequency domain, for both reflection and transmission measurements. Expected values for the wafers are included.

CHAPTER 5

5 Conclusions

5.1 Discussion

The thesis set out to characterize material parameters through reflection and transmission. The materials investigated thoroughly were: a one-layer PMMA sheet, a PMMA container, a silicon wafer and a thin gold film.

The material characterization was performed in two steps. First, the material to be measured upon was chosen and all relevant data, such as thickness of sample, distance from sample to antenna, reference sample etc. that could be obtained was collected. The second step consisted of simulating the measurement with one free parameter. These simulations were compared to measurements and material parameters, for example conductivity or permittivity, were extracted.

From the simulation pre-study section it became apparent that certain materials are easier to measure and extract material parameters from in either reflection or transmission. For example; the silicon in Figure 7 would be better to measure in transmission since there is a bigger difference in received magnitude over varying conductivities. In reflection it would be harder to discern a low conductivity from high conductivity silicon.

In a few cases there existed an angle difference between the measurements from time domain compared to frequency domain. This was the cause of the bad overlap between the time and frequency domain for the magnitude of the reflection in Figure 22 and the phase of the transmission in Figure 24. Special care therefore needs to be taken about positioning and angle accuracy of the sample. For the silicon-wafer in Figure 26 and Figure 27 the extrapolated value was quite off compared to the expected, see Table 2. This has to do with the fact that silicon gives approximately the same reflection or transmission over a certain conductivity span, see Figure 7. The expected resistivity value of $\rho = 4 - 7\ k\Omega cm$

corresponds to a conductivity of $\sigma = 0.014 - 0.025\, S/m$ which is within this conductivity range.

In the end it does not matter whether you perform the material characterization by using measurements from time domain or frequency domain, since once the data has been gathered it's just a matter of Fourier transform between them. Overall the method of material characterization by free space measurements seems to be a very promising area. Its possible applications within industry and the scientific community are wide and there is still more to explore. It is a young and hot topic within academics and some companies are already working on complete solutions, trying to turn them into profitable products.

5.2 Future work

The predicament with the sample not being perfectly perpendicular to the incoming electromagnetic wave is something that could be integrated into the fitting procedure. By sweeping the angle simultaneously as the material parameter of interest, a better match is achieved if an angle is present. This would however require a complete revision of the theory used since oblique incidences alter the reflection and transmission from an interface depending on the value of the angle. This kind of multi-variable optimization is the next logical step in further works. In this thesis only one parameter at a time was extracted. If one would instead sweep two or more variables, for example thickness, permittivity and angle, the fit might become even better. However, this poses the problem of exponentially increasing the computing time required. As the amount of variables increase, the number of iterations the simulation has to run through increases exponentially. This creates an upper limit on how many variables can be swept at the same time. The best way to combat this would be to keep the sweeping span very narrow for most parameters. Another difficulty of having many parameters is that it creates a global optimization problem; the program might find a very good fit but the correct one is outside the parameter sweep span.

Further materials that could be interesting to measure and apply the method on are solar cells and structured materials.

CHAPTER 6

6 Acknowledgements

I would like to thank my supervisors Professor Lars-Erik Wernersson and PhD student Sebastian Heunisch for providing help and guidance during the master's thesis. I would also like to thank Dr. Lars Ohlsson for letting me use his signal processing scripts and for proofreading/commenting on the master's thesis work.

CHAPTER 7

7 References

[1] Tzu-Yang Yu, Jose Alberto Ortega Oral Büyüköztürk, "A methodology for determining complex permittivity of construction materials based on transmission-only coherent, wide-bandwidth free-space measurements.," *Cement & Concrete Composites, ScienceDirect*, p. 11, 2006.

[2] Jerzy Krupka, "Frequency domain complex permittivity measurements at microwave frequencies," *IOPScience*, 2006.

[3] M.V.Jacob, J.Krupka C.D.Easton, "Non-destructive complex permittivity measurement of low permittivity thin film materials," *IOPScience, Measurement Science and Technology*, 2007.

[4] Sophocles J. Orfanidis, *Electromagnetic Waves and Antennas*.: Rutgers University, 2014.

[5] Martin Dressel and George Gruner, *Electrodynamics of Solids, Optical properties of Electrons in Matter*. Cambridge: Cambridge University Press, 2003.

[6] Chris Bishop, "The Relationship Between Loss, Conductivity, and Dielectric Constant," 2001.

[7] J. G. Chafee, "Method and apparatus for heating dielectric materials," 2,147,689.

[8] Loretta Jones Peter Atkins, *Chemical Principles; The quest for insight*, 5th ed. New York, United States of America: W. H. Freeman and Company, 2010.

[9] Göran Jönsson, *Våglära och Optik*. Lund, Sweden: Media-Tryck, 2010, pp. 12-

16.

[10] Raymond A. Serway, *Principles of Physics (2nd ed.)*. Fort Worth, Texas, 1998, p. 602.

[11] Mats Gustafsson Daniel Sjöberg, *Kretsteori, ellära och elektronik*. Lund, Sverige: KFS AB, 2013.

[12] Crish Bishop, "The Relationship Between Loss, Conductivity, and Dielectric Constant," 2001.

[13] Virginia Semiconductor, "The General Properties of Si, Ge, SiGe, SiO2 and Si3N4," Virginia Semiconductor , Fredericksburg, 2002.

[14] Sean C. Andrews, Steve Park, Julia Reinspach, Nan Liu, Michael F. Toney, Stefan C. B. Mannsfeld and Zhenan Bao Brian J. Worfolk, "Ultrahigh electrical conductivity in solution-sheared polymeric transparent films," *Proceedings of the National Academy of Sciences of the United States of America*, no. 112, 2015.

[15] Liangqi. Musumeci, Chiara. Jafari, Mohammad Javad. Ederth, Thomas. Inganäs, Olle Ouyang, "Imaging the Phase Separation Between PEDOT and Polyelectrolytes During Processing of Highly Conductive PEDOT:PSS Films," *ACS Applied Materials and Interfaces*, 2015.

[16] Lars Ohlsson, Lars-Erik Wernersson and Mats Gustafsson Iman Vakili, "Time-Domain System for Millimetre-Wave Material Characterization," Department of Electrical and Information Technology, Faculty of Engineering, LTH, Lund, 2015.

[17] Paul H. Young, *Electronic Communication Techniques, fifth edition*. Ohio: Pearson, 2004.

[18] W. Culshaw and M. Anderson, "Measurement of permittivity and dielectric loss with a millimetre-wave Fabry-Perot interferometer," *IEE Proc. Electron. Commun. Eng. pt. B*, vol. 109, no. 23, pp. 820-826, 1962.

[19] Milo W. Hyde IV and Michael J. Havrilla, "Measurement of Complex Permittivity and Permeability Using Two Flanged Rectangular Waveguides," *Air Force Institute of Technology*, 2007.

CHAPTER 8

8 Appendices

8.1 Source code

Design plots – one layer

```
clc
clear all
c0 = 3e8;
e0 = 8.854*10^-12;
f1 = 60*10^9;
lambda1 = c0./f1;
omega = 2*pi.*f1;
k = 2*pi./lambda1;
d = 300e-6;
% Conductivity vs permittivity
e1 = linspace(1.01,80,1000);
cond = logspace(-2,8,1000);
e2 = cond./(omega*e0);
[E1, C] = meshgrid(e1, cond);
[Gamma1, Tau1] = mesh_one_layer(d,k,e1,e2,cond);
figure(1);
FigHandle = figure(1);
set(FigHandle, 'Position', [50, 100, 1350, 470]);
subplot(1,2,1)
mesh(log10(C),E1, 20*log10(abs(Gamma1)));
ylabel('Re[\epsilon]', 'FontSize', 14); xlabel('logarithmic
cond (log(\sigma/(S/m)))', 'FontSize', 14);
zlabel('Reflectivity \Gamma (dB)', 'FontSize', 16)
title('Reflection', 'FontSize', 14);
colorbar; view([0 90]); caxis([-50 0]);
hold on
axis([min(log10(cond)) max(log10(cond)) e1(1) e1(end)])
subplot(1,2,2)
limit = 1e-10;
Tau1(abs(Tau1)<limit)=limit;
mesh(log10(C),E1, 20*log10(abs(Tau1)));
ylabel('Re[\epsilon]', 'FontSize', 14); xlabel('logarithmic
cond (log(\sigma/(S/m)))', 'FontSize', 14);
zlabel('Transmission \tau (dB)')
title('Transmission', 'FontSize', 14);
```

```
colorbar; view([0 90]); caxis([-50 0]);
axis([min(log10(cond)) max(log10(cond)) e1(1) e1(end)])

% Conductivity vs depth
e1 = linspace(1,1,1000);
d2 = logspace(-9,-3,1000);
[D2, C] = meshgrid(d2, cond);
[Gamma2, Tau2] = mesh_one_layer(D2,k,e1,e2,cond);
figure(2)
FigHandle = figure(2);
set(FigHandle, 'Position', [50, 100, 1350, 470]);
subplot(1,2,1)
mesh(log10(C),log10(D2),20*log10(abs(Gamma2)));
xlabel('logarithmic cond (log(\sigma/(S/m)))', 'FontSize',
14); ylabel('logarithmic Thickness (log(m/m))', 'FontSize',
14)
title('Reflection','FontSize', 14);
colorbar; view([0 90]); caxis([-50 0]);
subplot(1,2,2)
limit = 1e-10;
Tau2(abs(Tau2)<limit)=limit;
mesh(log10(C),log10(D2),20*log10(abs(Tau2)));
xlabel('cond (log(\sigma/(S/m)))', 'FontSize', 14);
ylabel('Thickness (log(m/m))', 'FontSize', 14)
title('Transmission','FontSize', 14);
colorbar; view([0 90]); caxis([-50 0]);


function [gamma, tau] = mesh_one_layer(d,k, e1, e2, cond)
n0 = ones(1000,1000);
[E11, E22] = meshgrid(e1, e2);
N = sqrt(E11 - 1i*E22);

p1 = (n0 - N)./(n0 + N);
p2 = (N - n0)./(N + n0);
t1 = 1 + p1;
t2 = 1 + p2;
z1 = exp(-2*1i*(N.*k).*d);
z2 = exp(-1i*(N.*k).*d);
tau = (t1.*t2.*z2)./(1 + p1.*p2.*z1);
gamma = (p1 + p2.*z1)./(1 + p1.*p2.*z1);

end
```

Design plots – two layer

```
clc
clear all
c0 = 3*10^8;
e0 = 8.854*10^-12;
f1 = 60*10^9;
lambda1 = c0./f1;
omega = 2*pi.*f1;
k = 2*pi./lambda1;
d = 300e-9;
d_Si = 300e-6;
e1 = linspace(1.01,80,1000);
cond = logspace(-2,8,1000);
e2 = cond./(omega*e0);
e_Si = 11.86 - 1i*((1/(6.4*10^2)))./(omega*e0);

% Meshplot
% Real permittivity vs real conductivity
[E1, C] = meshgrid(e1, cond);
[Gamma1, Tau1] = mesh_two_layers(d,d_Si,k,e1,e2,e_Si);
figure(1);
FigHandle = figure(1);
set(FigHandle, 'Position', [50, 100, 1350, 470]);
subplot(1,2,1)
mesh(log10(C),E1,20*log10(abs(Gamma1)));
axis([log10(min(cond)) log10(max(cond)) min(e1) max(e1)])
xlabel('logarithmic cond (log(\sigma/(S/m)))', 'FontSize',
14); ylabel('Re[\epsilon]', 'FontSize', 14)
title('Reflection','FontSize', 14)
colorbar; view([0 90]);

subplot(1,2,2)
mesh(log10(C),E1,20*log10(abs(Tau1)));
axis([log10(min(cond)) log10(max(cond)) min(e1) max(e1)])
xlabel('logarithmic cond (log(\sigma/(S/m)))', 'FontSize',
14); ylabel('Re[\epsilon]', 'FontSize', 14)
title('Transmission','FontSize', 14)
caxis([-50 0]); colorbar; view([0 90]);

e1 = linspace(10,10,1000);
d2 = logspace(-9,-6,1000);
[D2, C] = meshgrid(d2, cond);
[Gamma2, Tau2] = mesh_two_layers(D2,d_Si,k,e1,e2,e_Si);
figure(2)
FigHandle = figure(2);
set(FigHandle, 'Position', [50, 100, 1350, 470]);
subplot(1,2,1)
mesh(log10(C),log10(D2),20*log10(abs(Gamma2)));
```

```
xlabel('logarithmic cond (log(\sigma/(S/m)))', 'FontSize',
14); ylabel('logarithmic Thin-film thickness (log(m/m))',
'FontSize', 14)
title('Reflection','FontSize', 14)
view([0 90]);
colorbar;
subplot(1,2,2)
mesh(log10(C),log10(D2),20*log10(abs(Tau2)));
xlabel('logarithmic cond (log(\sigma/(S/m)))', 'FontSize',
14); ylabel('logarithmic Thin-film thickness (log(m/m))',
'FontSize', 14)
title('Transmission','FontSize', 14)
view([0 90]); caxis([-50 0]); colorbar;

% Real part vs depth (substrate)
d3 = logspace(-7,-3,1000);
[D3, cond] = meshgrid(d3, cond);
[Gamma3, Tau3] = mesh_two_layers(d,D3,k,e1,e2,e_Si);
figure(3)
FigHandle = figure(3);
set(FigHandle, 'Position', [50, 100, 1350, 470]);
subplot(1,2,1)
mesh(log10(C),D3./(10^-6),20*log10(abs(Gamma3)));
xlabel('logarithmic cond (log(\sigma/(S/m)))', 'FontSize',
14); ylabel('Substrate depth \mum', 'FontSize', 14)
title('Reflection','FontSize', 14)
caxis([-50 0]); view([0 90]); colorbar;
subplot(1,2,2)
mesh(log10(C),D3./(10^-6),20*log10(abs(Tau3)));
xlabel('logarithmic cond (log(\sigma/(S/m)))', 'FontSize',
14); ylabel('Substrate depth \mum', 'FontSize', 14)
title('Transmission','FontSize', 14)
caxis([-50 0]); view([0 90]); colorbar;

function [gamma, tau] =
mesh_two_layers(d_film,d_sub,k,e1,e2,e_sub)
[E11, E22] = meshgrid(e1, e2);
N0 = ones(1000,1000);
N1 = sqrt(E11 - 1i*E22);
N2 = sqrt(e_sub);
N2 = ones(1000,1000).*N2;
p1 = (N0 - N1)./(N0 + N1);
p2 = (N1 - N2)./(N1 + N2);
p3 = (N2 - N0)./(N0 + N2);
t1 = 1 + p1;
t2 = 1 + p2;
t3 = 1 + p3;
```

```
z1p = exp(1i*(N1.*k).*d_film);
z2p = exp(1i*(N2.*k).*d_sub);
z1n = exp(-1i*(N1.*k).*d_film);
z2n = exp(-1i*(N2.*k).*d_sub);
z1 = exp(-2*1i*(N1.*k).*d_film);
z2 = exp(-2*1i*(N2.*k).*d_sub);
gamma = (p1 + p2.*z1 + p1.*p2.*p3.*z2 + p3.*z1.*z2)./(1 +
p1.*p2.*z1 + p2.*p3.*z2 + p1.*p3.*z1.*z2);
tau = (t1.*t2.*t3)./(z1p.*z2p + p1.*p2.*z1n.*z2p +
p2.*p3.*z1p.*z2n + p1.*p3.*z1n.*z2n);
end
```

LUND
UNIVERSITY

Series of Master's theses
Department of Electrical and Information Technology
LU/LTH-EIT 2016-488

http://www.eit.lth.se